Ancillary Services of a Grid-Connected Inverter with Overcurrent Protection Capability under Voltage Sag

Sepannur Bandri*, Zuriman Anthony, Rafika Andari, and Fauzan Ismail

Department of Electrical Engineering, Padang Institute of Technology
Jl. Gajah Mada Kandis Nanggalo, Padang, 25173, Indonesia
**Corresponding author. Email: sepannur@itp.ac.id*

Abstract— The Distributed Generator of a Photovoltaic System (DGPVS) is an essential factor for future power plant generation, and it can be created by connecting multiple small power plant generators in a microgrid system. This paper focuses on the overcurrent protection of a three-phase grid-connected inverter (3P-GCI) under voltage sag conditions in sustaining connection loss between the 3P-GCI and the primary grid, which involves voltage instability. The ancillary service shows more advantage in overcurrent protection during voltage sags, which limits the generated current under sag duration. Its service can protect the inverter and avoid more disturbances to the primary grid because the 3P-GCI remains connected. Proposed LVRT strategy with limit current feature play the role to protect 3P-GCI under voltage sag. In the normal grid, the 3P-GCI can inject 302W of active power with a power factor (PF) equal to one. 1.4% of V_{THD} and 4.3% of I_{THD} shows the performance of the proposed system. Meanwhile, the 3P-GCI injects 239VAr reactive power and reduces injected active power to 135W which is essential to remain connected to the primary grid during voltage sags and limit the generated current. The validation results show that this prototype successfully compensates for the grid voltage drops by injecting 239Var of reactive power and limiting its generated current to 1.592A.

Keywords— active power; distribute generator; inverter; reactive power; voltage sag

I. INTRODUCTION

The future achievement of the Group of Twenty (G20) meeting forum has been focused on the zero net emissions of power system generator, which uses fossil fuel or coal as an energy raw material. As a member of G20, Indonesia should play the role and mandatory to reduce the usage of coal and fossil fuel for the electric power generator [1]. Alternatively, the photovoltaic system contributed as the distributed generator to support the primary power system [2]. Meanwhile, the challenge on the distributed generator for the Photovoltaics (PV) system should be intelligent and capable of sustaining when the primary power system generator is in the disturbance. Therefore, the distributed generator of the PV system with robust protection features must remain connected or disconnected from the primary power system.

The smart inverter design [3] considers the control strategy in several conditions of operational mode [4], [5]. Traditionally, in grid-connected operation, the injects active power into the primary grid and attempts to disconnect when the grid is under disturbances [6]–[8]. However, in advance, the smart inverter may be connected under grid voltage drop [9]–[12], utilize an anti-islanding protection algorithm [13]–[16], reactive power compensation [17], [18], active and reactive power injection [19], and even capable of sharing power with parallel connected inverter during islanding operational mode [17], [20], [21]. The overall strategy aims to enhance the inverter system protection to prevent instability [22]–[24].

Control strategies of the inverter can be configured by using a synchronous reference frame (*dq*-frame), stationary reference frame (αβ- frame), or natural reference frame (ABC-frame) [25], [26] where it can be a single loop, double loop, and a triple loop of controller [27], which generate the reference voltage of Space Vector Pulse Width Modulation (SVPWM) [28]. Every topology is operated with its advantage and challenges. The common inverter utilize the *dq*-frame and Proportional Integral (PI) controller with the main inner current control loop. Additional outer voltage and power control are possible based on the objective. Further, the inverter usually employ Maximum Power Point Tracking (MPPT) to achieve maximum power delivery. The maximum active power with zero reactive power is injected into the regular primary grid. This method experience with decreasing efficiency when the grid is under disturbance. Consequently, any protection method is employed during failure operation. Generally, over current protection is important to prevent the inverter system.

This paper presents the intelligent inverter with active and reactive power injection capabilities. The inner current and outer power loops are implemented to ensure power delivery. The MPPT strategy with a PI controller is used to control the DC-link voltage with the boost converter circuit. Meanwhile, low-voltage ride-through (LVRT) strategy include over-current protection is applied when the grid voltage drops to achieve a seamless voltage sag transition. The main contributions are summarized as follows:

- The inverter injects the active power with PF=1 into the normal grid.
- The inverter injects active and reactive power under grid voltage sag.
- The inverter applies over-current protection for the critical voltage sag to prevent the system.

The paper is organized as follows: Section 2 discusses the proposed system, configuration and control technique. Section 3 presents the prototype experiment, findings, and validation. Finally, Section 4 provides concluding remarks.

Received 12 April 2023, Revised 14 June 2023, Accepted 27 June 2023.
DOI: https://doi.org/10.15294/jte.v15i1.43870

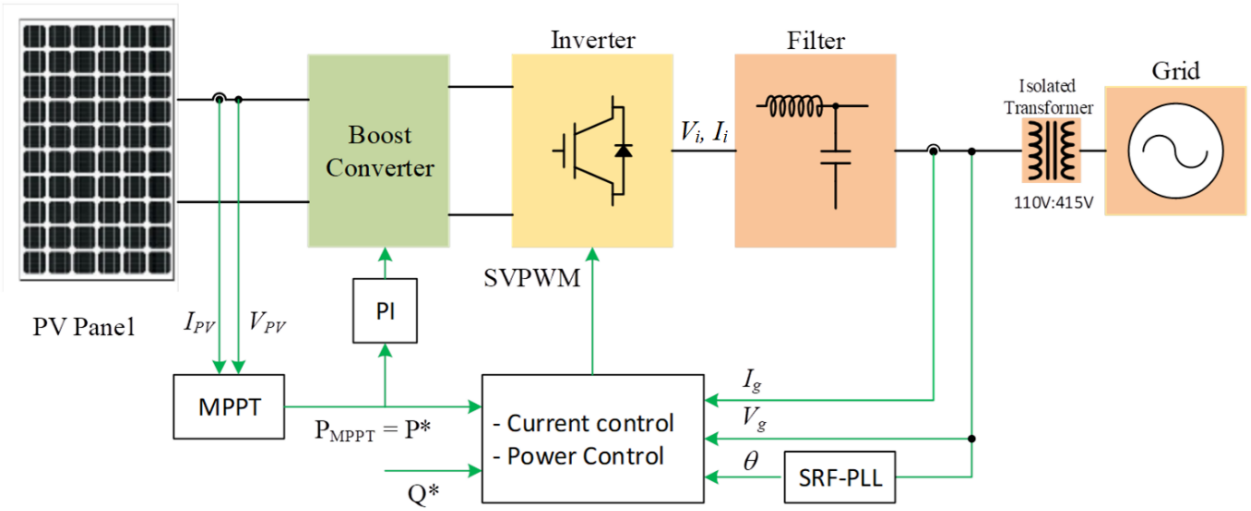

Figure 1. The DGPVS block diagram

II. METHOD

This section describes how the three-phase grid-connected inverter (3P-GCI) plays the role to support the function of the Distributed Generator of a Photovoltaic System (DGPVS). The 3P-GCI should decide its operating mode when the grid voltage drop happens. Figure 1 shows the block diagram of the 3P-GCI. Initially, by measured current and voltage of the PV panel that is denoted by I_{PV} and V_{PV}, respectively. Therefore, the active power reference (P^*) can be calculated by the MPPT method to define injected active power into the primary grid. Meanwhile, P^* is also used as a reference of generated power for the boost converter via the PI controller. In which boost converter is expected generate 300V DC, which supply the inverter. Another loop, Power controller and current controller are used to generate SVPWM to drive the six-switch of the inverter. As the feedback parameter, the inverter current, inverter voltage, and grid voltage are measured and denoted as I_i, V_i, and V_g, respectively.

TABLE I. PARAMETER OF THE GRID FEEDING INVERTER

Parameter	Value
The DG-rated voltage (V)	115
Filter inductance L_c (mH)	5
Filter capacitance (uF)	10
Switching frequency f_{sw} (kHz)	20
Rate frequency f (Hz)	50
Transformer ratio	115: 415
Output Boost Converter	300V DC
PV Panel @V_{mp} = 17.6V (Series, 10 x 100W)	V_{mp} =176V, I_{mp} = 5.69A

In the scenario, the inverter can be operated in grid-connected mode, Low Voltage Ride Through (LVRT) mode, and islanding mode based on the parameter listed in Table I. To achieve the grid code requirement, this 3P-GCI employs Synchronous Reference Frame Phase Lock Loop (SRF-PLL) method for synchronization. When the inverter meets the grid code, active power is injected into the grid equal to the P^* without generating the reactive power (Q). However, since the grid voltage drop less than 0.9 p.u from the nominal voltage, the 3P-GCI should detect the voltage sag with the Conventionally Synchronously Rotating Reference Frame (CSRRF) method. Then, calculate the required reference reactive current that should be injected to maintain the connection between the 3P-GCI and the grid. In addition, the 3P-GCI is operated under LVRT mode and is also possible to operate in islanding under severe voltage drop.

A. Proposed 3P-GCI model

The grid voltage, inverter voltage, and inverter current are denoted $V_{g_{(abc)}}$, $V_{i_{(abc)}}$, and $I_{i_{(abc)}}$, respectively. Therefore, the stationary a-b-c frame for voltage equations is expressed in (1).

$$\begin{aligned} V_{g_a} &= E\cos\omega t = -L_o\frac{dI_{i_a}}{dt} + V_{i_a} \\ V_{g_b} &= E\cos\left(\omega t - \frac{2}{3}\pi\right) = -L_o\frac{dI_{i_b}}{dt} + V_{i_b} \\ V_{g_c} &= E\cos\left(\omega t - \frac{4}{3}\pi\right) = -L_o\frac{dI_{i_c}}{dt} + V_{i_c} \end{aligned} \quad (1)$$

The maximum phase voltage, the angular frequency of the grid, and the inductance filter are denoted as E, ω, L_o, respectively. Therefore the stationary frame of the grid voltage (V_x and V_y) can be expressed in (2).

$$\begin{bmatrix} V_x \\ V_y \end{bmatrix} = \frac{2}{3}\begin{bmatrix} 1 & -\frac{1}{2} & -\frac{1}{2} \\ 0 & \frac{\sqrt{3}}{2} & -\frac{\sqrt{3}}{2} \end{bmatrix}\begin{bmatrix} V_{g_a} \\ V_{g_b} \\ V_{g_c} \end{bmatrix} = \begin{bmatrix} -L_o\frac{di_x}{dt} + v_x \\ -L_o\frac{di_y}{dt} + v_y \end{bmatrix} \quad (2)$$

Hence, the synchronous dq frame of the grid voltage is as follows:

$$\begin{bmatrix} V_d \\ V_q \end{bmatrix} = \begin{bmatrix} \cos(\omega t) & \sin(\omega t) \\ -\sin(\omega t) & \cos(\omega t) \end{bmatrix}\begin{bmatrix} V_x \\ V_y \end{bmatrix}$$

$$\begin{bmatrix} V_d \\ V_q \end{bmatrix} = \begin{bmatrix} \cos(\omega t) & \sin(\omega t) \\ -\sin(\omega t) & \cos(\omega t) \end{bmatrix}\left(-L_o\frac{d}{dt}\right).$$

$$\begin{bmatrix} \cos(\omega t) & \sin(\omega t) \\ -\sin(\omega t) & \cos(\omega t) \end{bmatrix}^{-1}\begin{bmatrix} I_d \\ I_q \end{bmatrix} + \begin{bmatrix} V_d \\ V_q \end{bmatrix}$$

$$\begin{bmatrix} V_d \\ V_q \end{bmatrix} = -L_o\frac{d}{dt}\begin{bmatrix} I_d \\ I_q \end{bmatrix} - \omega L_o\begin{bmatrix} -I_d \\ I_q \end{bmatrix} + \begin{bmatrix} V_d \\ V_q \end{bmatrix} \quad (3)$$

where V_d, V_q, I_d and I_q are d-axis of voltage, q-axis of voltage, d-axis of current, and q-axis of current, respectively. V_d equal to E and $V_q = 0$. To achieve the unity power factor, $I_q$should be controlled with zero reference $(i_q^* = 0)$. Therefore the injected active power to the primary grid is:

$$P = \frac{3}{2}(V_d I_d + V_q I_q) = \frac{3}{2}V_d I_d = \frac{3}{2}E i_d \quad (4)$$

Since the actual active power P is calculated in (4) and the reference active power $P^* = P_{mppt}$, the d-axis references current I_d^* in (5) is generated from the PI power controller as illustrated in Figure 2, which is expressed as:

$$I_d^* = k_p e + k_i \int e\, dt \quad (5)$$

$$e = P^* - P \tag{6}$$

and e is the error power between P^* and P.

The d-q frame of voltage equation (3) can be simplified as follows:

$$\begin{aligned} E &= -L_o \frac{dI_d}{dt} + \omega L_o I_q + V_d \\ 0 &= -L_o \frac{dI_q}{dt} - \omega L_o I_d + V_q \end{aligned} \tag{7}$$

In the inner current loop, the PI controller ensures that the actual and reference current error is close to zero. Equation (8) is used as effective decoupling control to improve the response.

$$\begin{aligned} V_d &= E - \omega L_o I_q + \Delta V_d \\ V_q &= \omega L_o I_d + \Delta V_q \end{aligned} \tag{8}$$

where ΔV_d and ΔV_q in (9) is required as additional voltage to maintain the sinusoidal input currents.

$$\begin{aligned} \Delta V_d &= k_{pd}(I_d^* - I_d) + k_{id} \int (I_d^* - I_d) dt \\ \Delta V_q &= k_{pq}\left(I_q^* - I_q\right) + k_{iq} \int \left(I_q^* - I_q\right) dt \end{aligned} \tag{9}$$

k_{pd} and k_{pq} are proportional control gain and k_{id} and k_{iq} are the integral control gain.

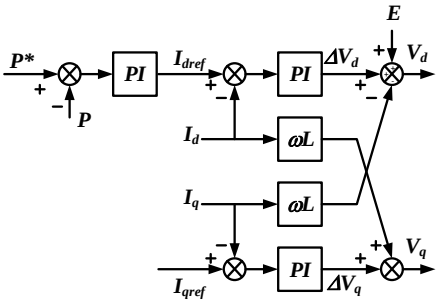

Figure 2. The control diagram of the 3P-GCI

B. Synchronous Reference Frame Phase-Lock-Loop (SRF-PLL)

Using a PLL, the voltage-source inverter is synchronized with the AC grid to inject power at the grid frequency. The PLL is a control system that generates an output signal with the same phase as the input signal and provides the rotating angle for the dq transformation to synchronize the converter control system with the grid frequency.

The specific PLL design depends on the requirements and applications. In Figure 3, the SRF-PLL block diagram displays V_{abc} as the measured three-phase voltages, and V_q is derived from Park's transformation and sent to a PI controller for additional processing. ω_{nom}, $\Delta\omega$, and ω represent the nominal angular frequency of the grid, the error of the angular frequency, and the estimated angular frequency, respectively, while θ represents the estimated phase angle of the grid voltage. This method can determine the grid voltage's frequency, phase angle, and magnitude for inverter output synchronization and controls [29].

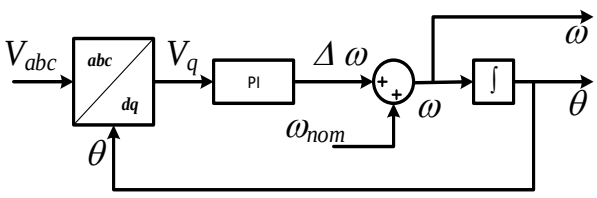

Figure 3. The diagram of SRF-PLL

C. The 3P-GCI under grid-connected mode

In the regular operation of the grid-connected mode, the inverter should follow the grid requirement for synchronization, as in Table II. Inverter may ensure the grid voltage and frequency is stable based on Table III. During Grid-connected mode, the inverter injected maximum active power with zero reactive power.

TABLE II. PARAMETER REQUIRED FOR SYNCHRONIZATION

Parameter	Required Range
Frequency difference	< 0.2 Hz
Voltage magnitude difference	< 10%
Voltage angle difference	< 10^o
Interlocking logic is satisfied	-

TABLE III. MINIMUM CONNECTION TIME FOR SYNCHRONIZATION

Voltage Level	Time
Low Voltage	2 minutes
Medium Voltage	5 minutes

D. The 3P-GCI under LVRT mode

Voltage sag, also known as a voltage dip, is a temporary reduction in the voltage level of an electrical system. A sudden increase in the current demand or a fault in the electrical system typically causes it. During a voltage sag, the voltage level drops below the normal operating range, which can cause equipment to malfunction or shut down. Voltage sags can have significant economic impacts, resulting in lost productivity, damaged equipment, and increased maintenance costs. Therefore, detecting and mitigating voltage sags is essential to maintaining electrical systems' reliability and stability. An illustration of the voltage sag can be shown in Figure 4.

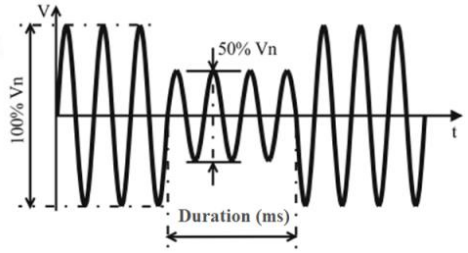

Figure 4. Voltage sag waveform

Figure 5 illustrates the voltage detection method based on the Conventionally Synchronously Rotating Reference Frame (CSRRF) [30]. This method detects voltage sag by utilizing the $abc - dq$ transformation to calculate DC quantities (V_d, V_q) proportion to AC quantities of the grid voltages (V_a, V_b, V_c) can be expressed as in (10).

$$\begin{bmatrix} V_d \\ V_q \end{bmatrix} = \frac{2}{3} \begin{bmatrix} \cos\omega t & -\sin\omega t \\ \sin\omega t & \cos\omega t \end{bmatrix} \begin{bmatrix} 1 & -1/2 & -1/2 \\ 0 & \sqrt{3}/2 & -\sqrt{3}/2 \end{bmatrix} \begin{bmatrix} V_a \\ V_b \\ V_c \end{bmatrix} \tag{10}$$

As mentioned in Figure 5, the sag signal is generated from a filtered $V_{dq} = \sqrt{V_d^2 + V_q^2}$ then compared to a DC reference in the comparator (i.e. 0.9pu). Where the V_{dq} varies related to measured grid voltage, and a Low Pass Filter (LPF) is utilized to eliminate 100Hz component or 2ω.

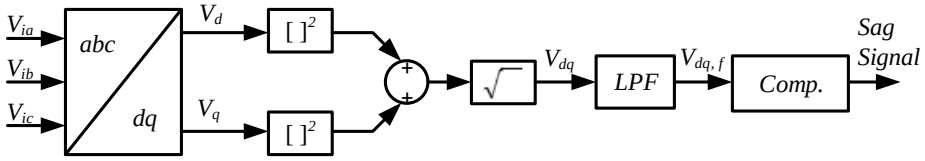

Figure 5. CSRRF-based voltage sag detection

Therefore, the LVRT strategy is used to prevent the distributed generator (DG) from the abnormal grid condition, where the grid voltage drops can influence the operational mode of the DG. Traditionally, the voltage sag condition forces the DG to operate in islanding or disconnected from the grid, which is capable to reconnect once the fault was resolved [6]–[8]. However, advanced microgrids attempt to maintain active power injection and provide reactive power injection during voltage sags [12]. As a result, the inverter system prevents instability [22]–[24].

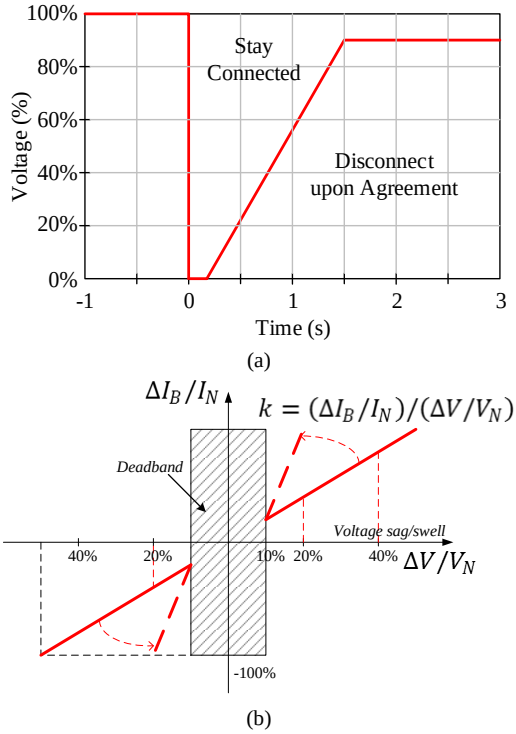

Figure 6. German grid code requirement (a) LVRT capability and (b) reactive power support capability

As demonstrated in Figure 6(a), the DGPVS are only permitted to disconnect from the grid when the grid voltage drops below the red curve. If not, the DGPVS must inject a specific quantity of reactive power, as shown in Figure 6(b). According to Figure 6(b), a 1% drop in grid voltage below $0.9V_N$ necessitates at least a k% increase in injected current. It should be able to provide 1p.u. of reactive current if necessary. The following are the related equations:

$$I_{q_{ref}} = \begin{cases} 0, & V_g > 0.9V_N \\ \left(-k.\frac{V_g}{V_N} + k\right) I_N, & 0.9V_N \geq V_g > 0.5V_N \\ I_N, & V_g \leq 0.5V_N \end{cases} \quad (11)$$

Where in (11), V_N represents the nominal grid voltage, I_N represents the rated current of the converter, ΔV represents the amount of voltage drop, and ΔI_B represents the increase in reactive current after a fault occurs. The German grid code [24] specifies that the constant k must be at least 2p.u.

Even in the event of faults in the grid, an advanced inverter that connects to the standard grid and provides active power while injecting reactive power must adhere to the grid code requirement [31]. The inverter should restrict its current during unusual operations to meet these standards. Therefore, the design of the inverter should take this into account.

$$\begin{cases} I_q = I_N, & 0 \leq v_g < \left(1 - \frac{1}{k}\right) p.u. \\ I_q = k(1 - v_g) I_N, & \left(1 - \frac{1}{k}\right) p.u. \leq v_g < 0.9\, p.u. \end{cases} \quad (12)$$

When there is a drop in grid voltage, the Reactive Power Injection (RPI) control is activated to inject reactive power as per the grid standards, such as the German grid code shown in Figure 6(a) [32]. The system must inject enough reactive current during fault ride-through operation under the grid voltage level [32]. The variables I_{q0} and v_g denote the initial reactive current before grid failure and the instantaneous voltage during voltage sag, respectively. Hence, the connection between these variables can be expressed in (13).

$$k = \frac{(I_q - I_{q0})/I_N}{(1 - v_g)}, \text{ωηεν } I_q < I_N \quad (13)$$

where $k \geq 2\ p.u.$

$$I_{g\,max} = \sqrt{I_d^2 + I_q^2} \leq I_{max} \quad (14)$$

In which, I_d represents the active current, $I_{g\,max}$ represents the injected currents amplitude, and I_{max} represents the maximum current level allowed by the inverter. The RPI strategies are proposed by (12) and (14).

The RPI strategies involving overcurrent loading can threaten inverters operating in LVRT (low voltage ride-through) modes. To avoid the risk of unintentional inverter shutdowns caused by overcurrent protection, the Const.-Ig max control strategy has been proposed. This approach ensures that the peak current injected from the grid remains constant and stays below the inverter current limit. In other words, $I_{g\,max} = nI_N = const.$, and $I_{g\,max} \leq I_{max}$, where n is the peak current scaling factor. By using (12), the current in the *dq*-frame can be expressed using the following formula when the grid voltage falls between the range of $\left(1 - (1/k)\right)p.u \leq V_g < 0.9p.u.$

$$\begin{cases} I_d = \sqrt{n^2 - k^2(1 - v_g)^2}\, I_N \\ I_q = k(1 - v_g) I_N \end{cases} \quad (15)$$

since the grid voltage drops lower than $\left(1 - (1/k)\right)p.u$, according to (14), the current in the *dq*-frame should be:

$$\begin{cases} I_d = \sqrt{n^2 - 1}\, I_N \\ I_q = I_N \end{cases} \quad (16)$$

The maximum value for n, which takes into account inverter current protection, is equal to $(I_{max}/I_N)p.u$ per unit. To ensure that the LVRT mode does not trip the inverter during stable RPI, the maximum value of n should be 2p.u if the inverter is designed with a margin of 2p.u (i.e., $I_{max} = 2I_N$). If n equals (I_{max}/I_N)., then the riding-through operation of the inverter will not amplify the injected grid current. In the meantime, LVRT will reduce the active power

according to (15) and (16) to allow for sufficient reactive power injection.

$$P = \frac{3}{2} V_{gm} I_d \quad (17)$$

where V_{gm} is the grid voltage amplitude.

E. The 3P-GCI under islanding mode

Islanding operation mode refers to the situation where a distributed power generation system (such as solar panels or wind turbines) continues to generate power even when the primary power grid has shut down. In other words, the distributed generation system *islands* itself and operates independently from the grid. This disturbance could happen when a sudden power outage, such as during a storm or other natural disaster, and the primary power grid no longer supplies the electricity. If the distributed power generation system is not designed to disconnect itself from the grid during a power outage, it may continue to generate power and supply it to the local area.

Islanding can be dangerous for several reasons, including the risk of electrocution for workers attempting to repair the primary power grid and the potential for damage to equipment or the grid itself. For this reason, power generation systems must be designed to detect islanding and shut down the power generation if it occurs. Islanding can also be intentional in some instances, such as in microgrids where a small community or facility is intentionally designed to operate independently from the primary power grid to improve reliability or reduce costs. In these cases, the distributed generation system is designed to detect when it needs to island itself and operate self-sufficiently.

Anti-islanding is a critical safety feature in distributed power generation systems. As mentioned earlier, islanding can occur when a distributed generation system continues to generate power even when the primary power grid has shut down. It can create a dangerous situation for workers attempting to repair the primary power grid and can also cause damage to the equipment or the grid itself. Anti-islanding is designed to prevent these situations by quickly detecting and disconnecting the distributed generation system from the grid if an islanding event occurs. The requirement standards are tabulated in Table IV [6].

There are several methods for implementing anti-islanding in distributed power generation systems. One common method is a frequency-based technique, where the system monitors the frequency of the power being supplied to the grid. If the frequency deviates too much from the normal range, the system will detect an islanding event and shut down power generation. Another method is a voltage-based technique, where the system monitors the voltage of the power being supplied to the grid. If the voltage deviates too much from the normal range, the system will detect an islanding event and shut down the power generation. These techniques can be combined to provide a more robust anti-islanding solution.

III. Results and Discussion

Figure 7 illustrates the proposed system, which is validated under laboratory experimental. A three-phase inverter is connected to the primary grid via a contactor switch and isolated transformer. The LCL filter is employed to filter the inverter output as a Pulse Width Modulation (PWM) reference. Furthermore, the inverter DC-Link is regulated by a conventional boost converter to maintain the DC voltage.

To achieve the synchronization requirement, initially, the controller measures the grid voltage and current, then calculates the amplitude of voltage, frequency and phase angle between voltage and current. The synchronization algorithm of the inverter should meet the rated voltage, frequency, and phase angle listed in Table II. The inverter waits for several minutes before being connected to the primary grid, following the minimum connection time in Table III. Here, the SRF-PLL method is used to generate a synchronized phase angle as shown in Figure 8(a). where the phase angle shown in CH1 involves the alignment of the inverter voltage V_i and grid voltage V_g. The inverter voltage, grid voltage, and phase angle frequency are 113V,112V, and 50Hz, respectively. Figure 8(b) shows the synchronization process of the measured signal and generated aligned inverter voltage against grid voltage. CH3 is a flag signal indicating inverter operation mode, 0 (low) means inverter is in stand-alone/islanding mode, and 1 (high) means grid-connected mode.

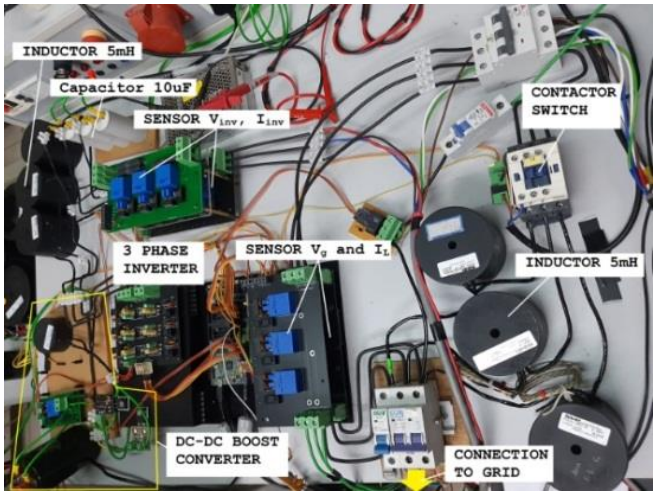

Figure 7. Prototype experimental configuration

TABLE IV. Existing Anti-Islanding Standards

Name of Standards	Quality factor, Q_f	Required islanding detection	Normal frequency range, f (nominal frequency f_o)	Normal voltage range, V (% of nominal voltage V_o)
IEC 62116	1	t<2s	$(f_0 - 1.5Hz) \leq f$ and $f \leq (f_0 + 1.5Hz)$	$85\% \leq V \leq 115\%$
IEEE 1547	1	t<2s	$59.3Hz \leq f \leq 60.5Hz$	$88\% \leq V \leq 110\%$
IEEE929-2000	2.5	t<2s	$59.3Hz \leq f \leq 60.5Hz$	$88\% \leq V \leq 110\%$
Japanese standard	0 (+rotating machinery)	passive: $t < 0.5s$ active: $0.5s < t < 1s$	Setting value	Setting value
Korean standard	1	t<0.5s	$59.3Hz \leq f \leq 60.5Hz$	$88\% \leq V \leq 110\%$
VDE 0126-1-1	2	t<0.2s	$47.5Hz \leq f \leq 50.2Hz$	$80\% \leq V \leq 115\%$
AS4777.3-2005	1	T<2s	Setting value	Setting value

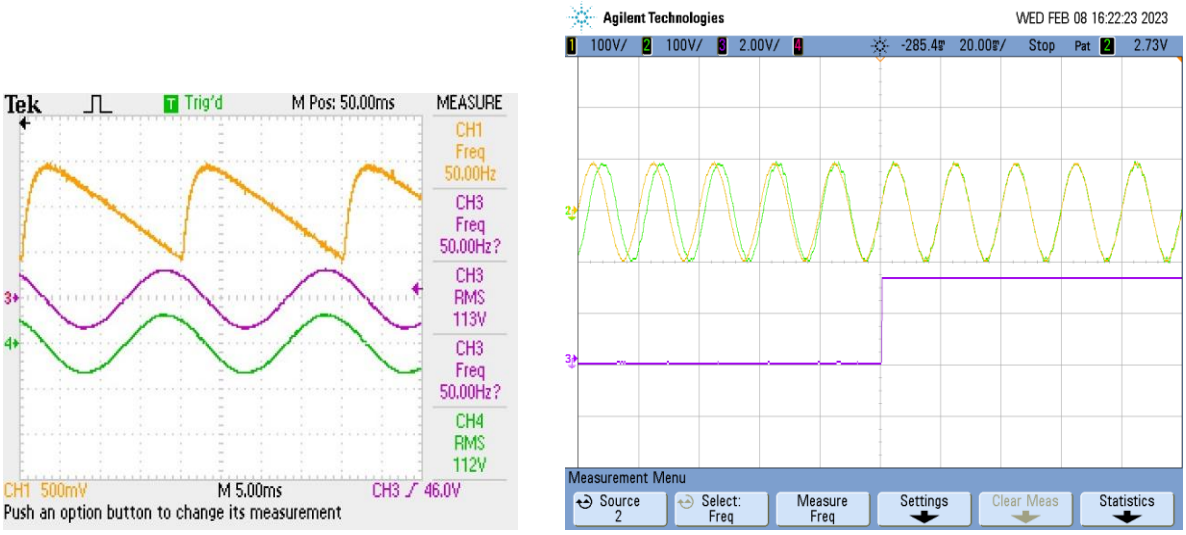

(a) (b)

Figure 8. Result for synchronization (a) phase angle and (b) transition process

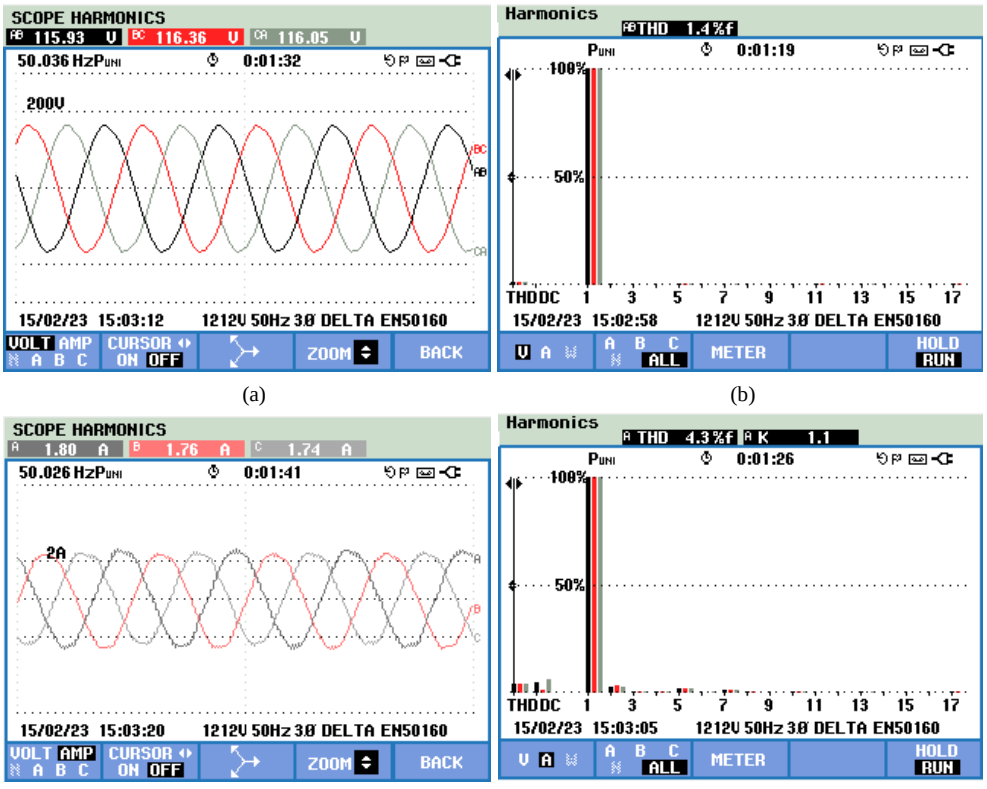

(a) (b)

(c) (d)

Figure 9. Performance of grid-connected inverter (a) V_{inv}, (b) V_{THD}, (c) I_{inv}, and (d) I_{THD}

The inverter is validated under grid-connected and voltage sag disturbances conditions. Figure 9 shows the inverter performance in the grid-connected mode of operation. 115V of balanced inverters voltage (in Figure 9(a)) and 1.8A of balanced inverters current (in Figure 9(c)) have been injected into the grid. The THD is measured by using the FLUKE 435-II Power Analyzer, which shows 1.4% of voltage harmonics V_{THD} and 4.3% of current harmonics I_{THD}. Therefore, this system can connect to the primary grid by following the grid-connected standard.

The inverter successfully injects 0.302 p.u (302W) of active power with 0VAr of reactive power to the primary grid. The inverter attempts to inject pure active power during the normal grid-connected mode. Otherwise, under voltage sag disturbance, the inverter injects some reactive power to compensate for the situation. Consequently, the inverter should be capable of handling voltage sag disturbance. The result of the LVRT strategy to apply for overcurrent protection during the grid voltage drop is shown in Figure 10. Limit current control has been implemented in this experiment. The inverter holds the limit current during normal either voltage sag disturbance.

Based on the experiment, the grid voltage drops from 65.77V to 50.70V. As defined that 66V is equal to 1.0 pu, therefore the grid voltage drops falls to 0.77pu during 0.4s. There isn't a spike-up current in the falling-edge transition when voltage sag happened, and also seamless during recovery time to normal. A peak current control strategy can maintain the maximum allowable injection current to the primary grid during voltage sag. Under voltage sag conditions, the inverter current look lagging more than 60^o than the voltage. The impacts are shown that active power decreased from 0.302p.u (302W) to 0.135p.u (135W), and reactive power increasing from 0p.u (0VAr) to 0.239p.u (239VAr).

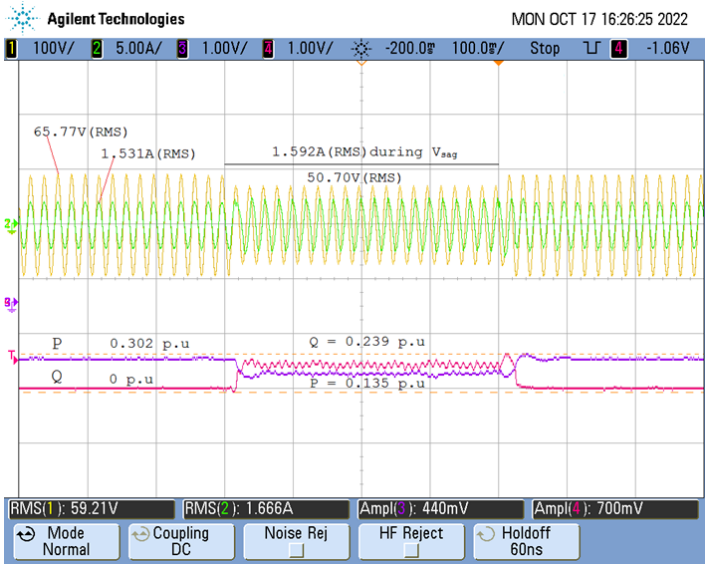

Figure 10. Peak current control during voltage sag (k=2, and n = 0.5) (CH1: V_g, CH2: I_i, CH3: P, CH4: Q)

TABLE V. COMPARISON TECHNIQUE CURRENT LIMITATION STRATEGY FOR THE DISTRIBUTED GENERATOR

Author, Year	Method	Power Injection	Sag Transition	Recovery time	Control System	Loop Control
[26], 2017	HDCS	P and Q	spike-up	Less than 0.01s	OPAL RT	Power Loop + Voltage Loop + Current Loop
[32], 2013	Instantaneous power theory	P and Q	0.02 delay	More than 0.12s	TMS320C6711 DSP	Power Loop + Current Loop
[22], 2019	FCHL	P and Q	seamless	Less than 0.02s	MATLAB	Current loop (PR control)
[11], 2020	AMPC	P and Q are not declare	seamless	Less than 0.01s	dSPACE - CP1103	Current loop
[33], 2019	Active Current Limiting	P and Q	spike-up	More than 0.1s	MATLAB	Current loop
Proposed	Peak Current Control	P and Q	seamless	Less than 0.01s	DSP F28335	Power Loop + Current Loop

HDCS : Hierarchical Droop Control Strategy.
PCC : Peak Current Control.
FCHL : Fault Current Hierarchical Limitation
AMPC : Autonomous Model Predictive Control

Table V have been listed a comparison of several methods in handling voltage sag with the current limit strategy. There are five compared methods discussed in their performance. In general, the LVRT method is related to the RPI to support grid voltage drop. However, reference [11] is not discussed and explains P and Q injection to the primary grid. Two methods by reference [26] and [33] show the current and voltage spike in the transition of voltage sag, which can affect the performance of the generated power. The method by the reference [32] shows the delay in the transition of a voltage sag with a long recovery time. Meanwhile, the seamless sag transition is presented by [22] and [11]. However, the reference [22] only simulates the method by using MATLAB and the reference [11] does without a quantitative explanation for the injected active and reactive power. Consequently, the author proposed the Peak Current Control for the LVRT strategy to handle grid voltage sag. Utilization of the power loop and current loop provides the effect for proportional active and reactive power injection. Therefore, the proposed method looks seamless in the sag transition, and with fast recovery time than other methods. The experiment can be ensured that the proposed peak current control is successful in protecting the inverter during voltage sag.

IV. CONCLUSION

The proposed grid-connected inverter is successfully operating under regular and grid disturbances. Under a normal grid, the inverter inject 302W of active power with 0VAr of reactive power. The proposed synchronization scenario can be executed well. The inverter voltage and current are regulated and aligned with the grid voltage. When the voltage sag happens, the inverter attempts to inject the amount of reactive power into the primary grid to sustain the power flow from the inverter. The LVRT has been validated to maintain the connection between inverter and grid during voltage sag. Increasing injected reactive power to 239VAr and reducing injected active power to 135W is caused by 60^o of shifting current related to the required active and reactive current injection during grid voltage sag. The inverter has response to voltage sag with seamless transition and fast recovery time (0.01s) compared to other method. Finally, the experimental test validates the prototype of the proposed inverter with embedded limit current control. It was capable of maintaining the limit current during grid voltage drop. As a trend of future research, other parameters such as grid frequency and grid impedance can be considered in handling grid disturbance.

REFERENCES

[1] K. Handayani and P. Anugrah, "Assessing the implications of net-zero emissions pathways: An analysis of the Indonesian power sector," *ICT-PEP 2021 - International Conference on Technology and Policy in Energy and Electric Power: Emerging Energy Sustainability, Smart Grid, and Microgrid Technologies for Future Power System, Proceedings*, pp. 270–275, 2021, doi: 10.1109/ICT-PEP53949.2021.9600954.

[2] Y. Zhou *et al.*, "Application of Distributed Ledger Technology in Distribution Networks," *Proceedings of the IEEE*, vol. 110, no. 12, pp. 1963–1975, 2022, doi: 10.1109/JPROC.2022.3181528.

[3] X. Zhao, L. Chang, R. Shao, and K. Spence, "Power System Support Functions Provided by Smart Inverters—A Review," *CPSS Transactions on Power Electronics and Applications*, vol. 3, no. 1, pp. 25–35, 2018.

[4] T. S. Ustun, K. Otani, Y. Aoto, and J. U. N. Hashimoto, "Optimal PV-INV Capacity Ratio for Residential Smart Inverters Operating Under Different Control Modes," *IEEE Access*, vol. 8, 2020, doi: 10.1109/ACCESS.2020.3003949.

[5] J. Joshi, A. K. Swami, V. Jately, and B. Azzopardi, "A Comprehensive Review of Control Strategies to Overcome Challenges during LVRT in PV Systems," *IEEE Access*, vol. 9, pp. 121804–121834, 2021, doi: 10.1109/ACCESS.2021.3109050.

[6] F. Wang, J. L. Duarte, and M. A. M. Hendrix, "Pliant active and reactive power control for grid-interactive converters under unbalanced voltage dips," *IEEE Trans Power Electron*, vol. 26, no. 5, pp. 1511–1521, 2011, doi: 10.1109/TPEL.2010.2052289.

[7] IEEE Standard 1547, *IEEE Standard for Interconnecting Distributed Resources with Electric Power Systems*. 2003.

[8] M. R. Islam and H. A. Gabbar, "Study of Micro Grid Safety & Protection Strategies with Control System Infrastructures," *Smart Grid and Renewable Energy*, vol. 3, no. 1, pp. 1–9, 2012, doi: 10.4236/sgre.2012.31001.

[9] B. Mirafzal, "On Grid-Interactive Smart Inverters : Features and Advancements," *IEEE Access*, vol. 8, pp. 160526–160536, 2020, doi: 10.1109/ACCESS.2020.3020965.

[10] M. M. Koutenaei, G. S. Member, and T. Nguyen, "Efficient Phasor-Based Dynamic Volt / VAr and Volt / Watt Analysis of Large Distribution Grid With High Penetration of Smart Inverters," *IEEE Trans Smart Grid*, vol. 13, no. 5, pp. 3997–4008, 2022, doi: 10.1109/TSG.2021.3138741.

[11] R. Capability, M. Easley, S. Member, S. Jain, and M. Shadmand, "Autonomous Model Predictive Controlled Smart Inverter With Proactive Grid Fault," vol. 35, no. 4, pp. 1825–1836, 2020, doi: 10.1109/TEC.2020.2998501.

[12] F. Ismail, A. Effendi, and W. Witrionanda, "Power Injection on Single Phase Grid System," *Elkha*, vol. 11, no. 1, p. 47, 2019, doi: 10.26418/elkha.v11i1.30932.

[13] D. Pal, B. K. Panigrahi, and S. Member, "Small Signal Stability Analysis Oriented Design of Hybrid Anti-Islanding Protection Technique Based on Active Disturbance Injection," *IEEE Syst J*, vol. 16, no. 1, pp. 1448–1459, 2022, doi: 10.1109/JSYST.2021.3050468.

[14] D. Motter and J. Vieira, "Influence of a Step-Voltage Regulator on Synchronous DG Anti-Islanding Protection," *IEEE Latin America Transactions*, vol. 17, no. 6, pp. 897–906, 2019.

[15] C. M. Vieira, "Hardware Implementation and Real-Time Evaluation of an ANN-Based Algorithm for Anti-Islanding Protection of Distributed Generators," *IEEE Transactions on Industrial Electronics*, vol. 65, no. 6, pp. 5051–5059, 2018, doi: 10.1109/TIE.2017.2767524.

[16] O. Raipala, S. Member, A. S. Mäkinen, S. M. Ieee, and S. Repo, "An Anti-islanding Protection Method Based on Reactive Power Injection and ROCOF," *IEEE Transactions on Power Delivery*, vol. 32, no. 1, pp. 401–410, 2017, doi: 10.1109/TPWRD.2016.2543503.

[17] A. M. Dissanayake, S. Member, and N. C. Ekneligoda, "Transient Optimization of Parallel Connected Inverters in Islanded AC Microgrids," *IEEE Trans Smart Grid*, vol. 10, no. 5, pp. 4951–4961, 2019, doi: 10.1109/TSG.2018.2871413.

[18] W. Liang, Y. Liu, and Y. Shen, "Active Power Control Integrated With Reactive Power Compensation of Battery Energy Stored Quasi-Z Source Inverter PV Power System Operating in VSG Mode," *IEEE J Emerg Sel Top Power Electron*, vol. 11, no. 1, pp. 339–350, 2023, doi: 10.1109/JESTPE.2021.3137397.

[19] D. I. Brandao, F. E. G. Mendes, R. V. Ferreira, S. M. Silva, and I. A. Pires, "Active and reactive power injection strategies for three-phase four-wire inverters during symmetrical/asymmetrical voltage sags," *IEEE Trans Ind Appl*, vol. 55, no. 3, pp. 2347–2355, 2019, doi: 10.1109/TIA.2019.2893135.

[20] A. Rosini, A. Labella, A. Bonfiglio, R. Procopio, and J. M. Guerrero, "A review of reactive power sharing control techniques for islanded microgrids," vol. 141, no. May 2020, 2021.

[21] H. Liu *et al.*, "Seamless Transfer Scheme With Unified Control Core for Paralleled Systems," *IEEE Trans Power Electron*, vol. 34, no. 7, pp. 6286–6298, 2019.

[22] X. Liu *et al.*, "Fault Current Hierarchical Limitation Strategy for Fault Ride-Through Scheme of Microgrid," *IEEE Trans Smart Grid*, vol. 10, no. 6, pp. 6566–6579, 2019, doi: 10.1109/TSG.2019.2907545.

[23] A. Khoshooei, J. S. Moghani, I. Candela, and P. Rodriguez, "Control of D-STATCOM during Unbalanced Grid Faults Based on DC Voltage Oscillations and Peak Current Limitations," *IEEE Trans Ind Appl*, vol. 54, no. 2, pp. 1680–1690, 2018, doi: 10.1109/TIA.2017.2785289.

[24] X. Zhao, J. M. Guerrero, M. Savaghebi, J. C. Vasquez, X. Wu, and K. Sun, "Low-voltage ride-through operation of power converters in grid-interactive microgrids by using negative-sequence droop control," *IEEE Trans Power Electron*, vol. 32, no. 4, pp. 3128–3142, 2017, doi: 10.1109/TPEL.2016.2570204.

[25] N. Bottrell and T. C. Green, "Comparison of current-limiting strategies during fault ride-through of inverters to prevent latch-up and wind-up," *IEEE Trans Power Electron*, vol. 29, no. 7, pp. 3786–3797, 2014, doi: 10.1109/TPEL.2013.2279162.

[26] H. R. Baghaee, M. Mirsalim, G. B. Gharehpetian, and H. A. Talebi, "A new current limiting strategy and fault model to improve fault ride-through capability of inverter interfaced DERs in autonomous microgrids," *Sustainable Energy Technologies and Assessments*, vol. 24, pp. 71–81, 2017, doi: 10.1016/j.seta.2017.02.004.

[27] Q. Liu, T. Caldognetto, and S. Buso, "Review and Comparison of Grid-Tied Inverter Controllers in Microgrids," *IEEE Trans Power Electron*, vol. 35, no. 7, pp. 7624–7639, 2020, doi: 10.1109/TPEL.2019.2957975.

[28] L. Di Benedetto *et al.*, "A Hardware Architecture for SVPWM Digital Control With Variable Carrier Frequency and Amplitude," *IEEE Trans Industr Inform*, vol. 18, no. 8, pp. 5330–5337, 2022.

[29] Y. Li, Y. Gu, S. Member, and T. C. Green, "Revisiting Grid-Forming and Grid-Following Inverters : A Duality Theory," *IEEE Transactions on Power Systems*, vol. 37, no. 6, pp. 4541–4554, 2022, doi: 10.1109/TPWRS.2022.3151851.

[30] Y. Kumsuwan and Y. Sillapawicharn, "A fast synchronously rotating reference frame-based voltage sag detection under practical grid voltages for voltage sag compensation systems," *IET Conference Publications*, vol. 2012, no. 592 CP, 2012, doi: 10.1049/cp.2012.0348.

[31] Y. Yang, H. Wang, and F. Blaabjerg, "Reactive power injection strategies for single-phase photovoltaic systems considering grid requirements," *IEEE Trans Ind Appl*, vol. 50, no. 6, pp. 4065–4076, 2014, doi: 10.1109/TIA.2014.2346692.

[32] Y. Bae, T. K. Vu, and R. Y. Kim, "Implemental control strategy for grid stabilization of grid-connected PV system based on German grid code in symmetrical low-to-medium voltage network," *IEEE Transactions on Energy Conversion*, vol. 28, no. 3, pp. 619–631, 2013, doi: 10.1109/TEC.2013.2263885.

[33] R. Ntare, N. H. Abbasy, and K. H. M. Youssef, "Low Voltage Ride through Control Capability of a Large Grid Connected PV System Combining DC Chopper and Current Limiting Techniques," *Journal of Power and Energy Engineering*, vol. 7, no. 1, pp. 62–79, 2019, doi: 10.4236/jpee.2019.71004.